Three-Dimensional Instabilities in Flow Past a Rotating Cylinder

S. Mittal
Department of Aerospace Engineering,
Indian Institute of Technology,
Kanpur, UP 208 016, India
e-mail: smittal@iitk.ac.in

Flow past a spinning circular cylinder placed in a uniform stream is investigated via three-dimensional computations. A stabilized finite element method is utilized to solve the incompressible Navier-Stokes equations in the primitive variables formulation. The Reynolds number based on the cylinder diameter and freestream speed of the flow is 200. The nondimensional rotation rate, α, (ratio of the surface speed and freestream speed) is 5. It is found that although the two-dimensional flow for $\alpha=5$ is stable, centrifugal instabilities exist along the entire span in a three-dimensional set-up. In addition, a "no-slip" side-wall can result in separation of flow near the cylinder ends. Both these effects lead to a loss in lift and increase in drag. The end conditions and aspect ratio of the cylinder play an important role in the flow past a spinning cylinder. It is shown that the Prandtl's limit on the maximum lift generated by a spinning cylinder in a uniform flow does not hold. [DOI: 10.1115/1.1631032]

1 Introduction

One of the earliest experiments for flow past a rotating cylinder were carried out by Prandtl [1]. He argued that the maximum lift generated by a spinning cylinder in a uniform flow is limited to 4π ($\sim$12.6). He also studied the effect of end conditions and aspect ratio. An increase in the overall lift coefficient was observed by utilizing end plates and using cylinders of higher aspect ratio. Since then, various studies have been conducted.

Recently, two-dimensional simulations for flow past a rotating cylinder have been presented by Mittal and Kumar [2]. The Reynolds number based on the cylinder diameter and freestream speed is 200 and various spin rates ($0\leqslant\alpha\leqslant5$) are considered. Here, α is the nondimensional rotation rate of the cylinder and is given as $\alpha=a\omega/U$ where U is the freestream speed and ω is the angular velocity of the cylinder about its own axis. For $0\leqslant\alpha\leqslant1.9$ a von Karman street is seen in the wake behind the cylinder. For nonzero α the vortex street is deflected away from the center line. The wake becomes narrower and the Strouhal number for vortex shedding decreases with increase in rotation rate. Vortex shedding ceases beyond $\alpha\sim1.9$. At high rotation rates it is seen that the lift for purely two-dimensional flows can be very large. The values of the lift coefficient obtained in the present work exceed the maximum limit based on the arguments of Prandtl. The flow remains stable for $1.91\leqslant\alpha\leqslant4.34$ but looses its stability, again, for $\alpha\sim4.35$. For this rotation rate, unlike the shedding for lower α, the cylinder sheds vortices of counterclockwise sense only from its lower surface. Vortex shedding continues for higher spin rates and the flow becomes stable, yet again, for $\alpha\geqslant4.8$. This was confirmed by carrying out a linear stability analysis of the flow. A possible cause for this interesting behavior of flow stability was also proposed.

One of the issues that remains unresolved is the maximum lift that can be generated by a rotating cylinder placed in a uniform flow. Researchers in the past have reported varied results on the magnitude of lift that can be generated via the Magnus effect. Goldstein [3], based on intuitive arguments by Prandtl, suggests that the maximum value of the lift coefficient that can be generated by a spinning cylinder is 4π ($\sim$12.6). The measurement of lift on a rotating cylinder is quite difficult due to the limitations posed by the rotation of the cylinder. Tokumaru and Dimotakis [4] devised a method to estimate the mean lift acting on a rotating cylinder in uniform flow. It is based on an inviscid point-vortex model and the transverse velocity that is measured, experimentally, ahead of the cylinder. Their results for $\mathrm{Re}=3.8\times10^3$ show that Prandtl's limit on lift coefficient ($C_{L_{\max}}=4\pi$) can be exceeded. For example, for $\alpha=10$ and a cylinder with span to diameter ratio of 18.7, they report an estimated lift coefficient that is more than 20% larger than this limit. Further, the trend of results suggests that C_L can made larger for higher rotation rates and by taking cylinders of larger aspect ratio. They have suggested that perhaps it is the unsteady effects that weaken Prandtl's hypothesis and that the three-dimensional/end effects are responsible for lowering the value of lift coefficient that could be achieved in a purely two-dimensional flow. However, Chew et al. [5] have reported that their two-dimensional computations are in agreement with Prandtl's postulate. They find that for $\mathrm{Re}=1000$, the estimated mean lift coefficient approaches asymptotic values with increase in α. At $\alpha=6$ they predict a mean lift coefficient of 9.1. Glauert [6] proposed a solution for a cylinder spinning at high rotation rates where the separation is suppressed. The solution of the flow in the boundary layer is obtained in the form of a power series and an expression for the circulation on the cylinder is obtained. Glauert found that Prandtl's limit can be exceeded and that the circulation increases indefinitely with α. The assumed model for the flow is valid only for those values of α when the flow separation is suppressed.

Most of the other investigations have been limited to $\alpha\leqslant3.25$. Chen et al. [7] computed flow for $\mathrm{Re}=200$ and $\alpha\leqslant3.25$. Their computation for $\alpha=3.25$ does show C_L whose instantaneous value exceeds 4π, marginally. However, they report results only for $t\leqslant24$. Computations by Badr et al. [8] for $\alpha=3$ and $\mathrm{Re}=1000$ are limited to $t\leqslant22$. At $t=22$ C_L is 8.8, approximately, and the trend of their results suggest higher C_L for larger times. The drag coefficient, C_D, reaches almost a steady-state value of 5.2. The mean values for C_D and C_L for the fully developed flow reported by Chew et al. [5], for $\alpha=3$, are 2.8 and 8.7, respectively. Recently, Chou [9] has also reported computational results for this flow problem. The time histories of C_D and C_L from his computations, for $\mathrm{Re}=1000$ and $\alpha=3$, match quite well with those from Badr et al. [8] for early times. However, for $t>5$, he reports much larger values of C_L and smaller values of C_D. It is interesting to observe that the streamline patterns from all the three sets of computations are quite similar and are in good agreement with the flow visualization results. Yet, the discrepancy

Contributed by the Applied Mechanics Division of THE AMERICAN SOCIETY OF MECHANICAL ENGINEERS for publication in the ASME JOURNAL OF APPLIED MECHANICS. Manuscript received by the Applied Mechanics Division, December 18, 2002; final revision, April 21, 2003. Associate Editor: T. E. Tezduyar. Discussion on the paper should be addressed to the Editor, Prof. Robert M. McMeeking, Chair, Department of Mechanics and Environmental Engineering, University of California–Santa Barbara, Santa Barbara, CA 93106-5070, and will be accepted until four months after final publication in the paper itself in the ASME JOURNAL OF APPLIED MECHANICS.

in the time histories of the aerodynamic coefficients is quite large. Our results for $\alpha=5$ for various Re, reported in earlier articles Mittal [10,11] result in large values of C_L. Recently, Stansby and Rainey [12] have reported computational results for Re=200 and $0\leqslant\alpha\leqslant5$. They observe an unsteady flow for lower rotation rates. For high rotation rates a steady flow with very large C_L is realized.

Results are presented for three-dimensional computations past a finite cylinder for various aspect ratios and with different end conditions. One of the objectives of the computations is to investigate the existence of three-dimensional instabilities in the flow for $\alpha=5$. We also wish to study the effect of end conditions. It has been observed in experiments that the use of end plates can lead to a substantial increase in lift generated by the cylinder. The present

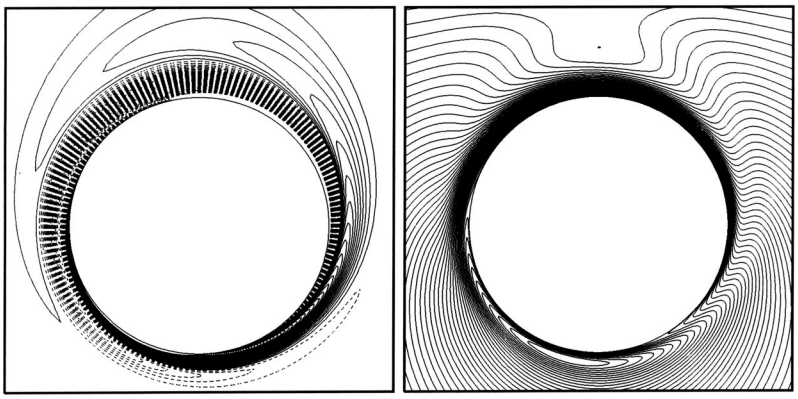

Fig. 1 Re=200, $\alpha=5$ flow past a rotating cylinder: closeup view of the vorticity (left) and magnitude of velocity (right) for the fully developed two-dimensional flow. The freestream flow is from left to right and the cylinder is rotating in a counterclockwise sense. Solid lines denote positive while the broken lines show negative vorticity.

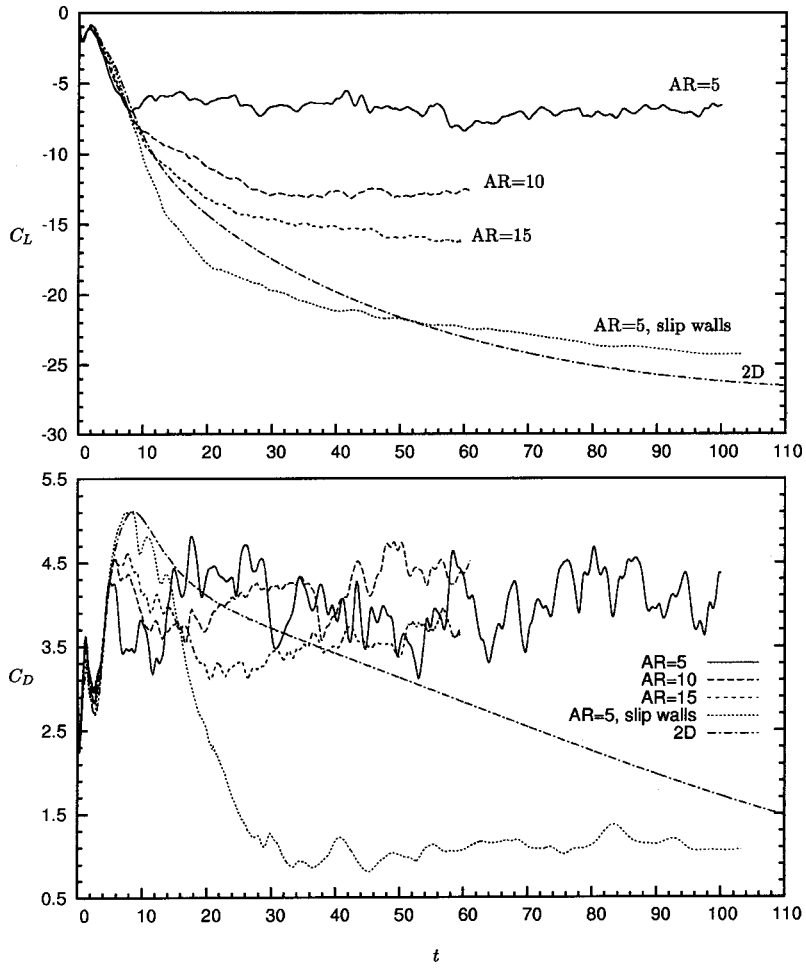

Fig. 2 Re=200, $\alpha=5$ flow past a rotating cylinder: time histories of the lift and drag coefficients for two-dimensional and three-dimensional computations with cylinders of various aspect ratios (*AR*)

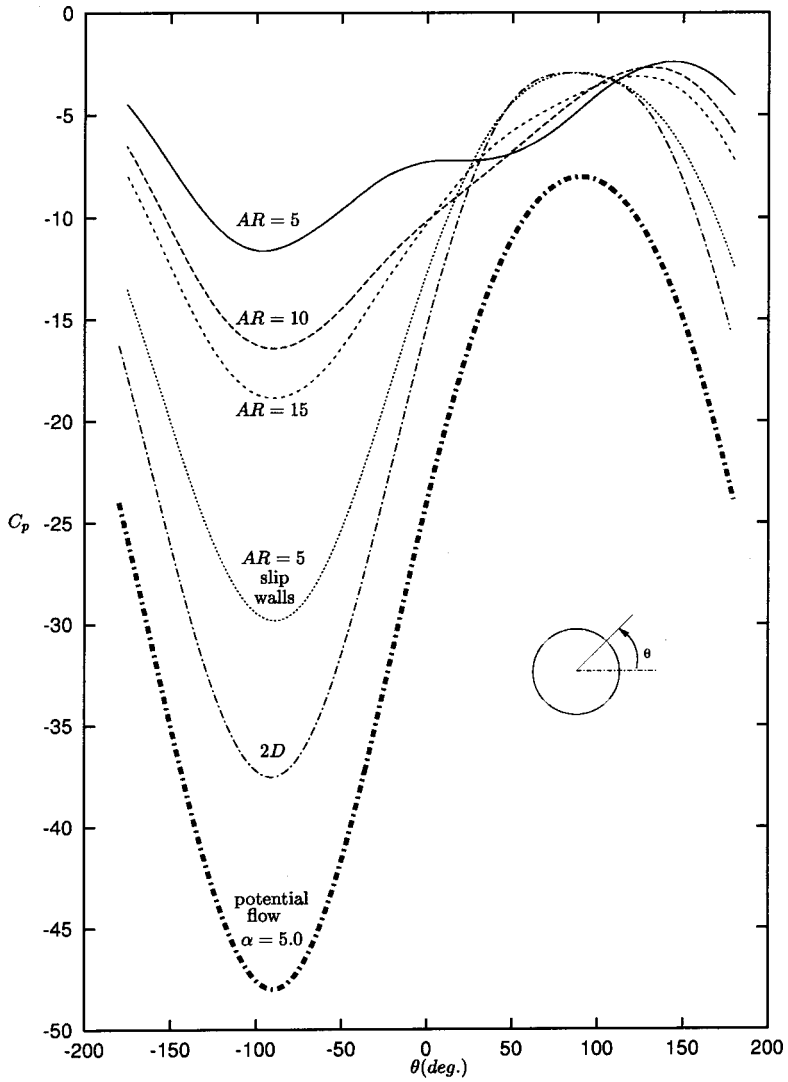

Fig. 3 Re=200, α=5 flow past a rotating cylinder for various aspect ratios: variation of the spanwise averaged pressure coefficient on the surface of cylinder

computations show that flow for Re=200 and $\alpha=5$ is associated with centrifugal instabilities that exist along the span of the spinning cylinder. Further, in the presence of a "no-slip" side wall the flow near the wall separates leading to unsteadiness in the wake. As expected, the effect is more drastic for low aspect-ratio cylinders. It is the end wall and aspect-ratio effects that limit the lift generated via Magnus effect.

The outline of the rest of the article is as follows. We begin by reviewing the governing equations for incompressible fluid flow in Section 2. The problem setup is defined along with the boundary and initial conditions. The SUPG (streamline-upwind/Petrov-Galerkin) and PSPG (pressure-stabilizing/Petrov-Galerkin) stabilization technique, [13], is employed to stabilize our computations against spurious numerical oscillations and to enable us to use equal-order-interpolation velocity-pressure elements. Section 3 describes the finite element formulation incorporating these stabilizing terms. In Section 4 computational results for flows involving rotating cylinder are presented and discussed. In Section 5 a few concluding remarks are made.

2 The Governing Equations

Let $\Omega\subset\mathbb{R}^{n_{sd}}$ and $(0,T)$ be the spatial and temporal domains respectively, where n_{sd} is the number of space dimensions, and let Γ denote the boundary of Ω. The spatial and temporal coordinates are denoted by $\mathbf{x}$ and t. The Navier-Stokes equations governing incompressible fluid flow are

$$\rho\left(\frac{\partial\mathbf{u}}{\partial t}+\mathbf{u}\cdot\nabla\mathbf{u}-\mathbf{f}\right)-\nabla\cdot\boldsymbol{\sigma}=0 \quad \text{on } \Omega \text{ for } (0,T), \tag{1}$$

$$\nabla\cdot\mathbf{u}=0 \quad \text{on } \Omega \text{ for } (0,T). \tag{2}$$

Here ρ, $\mathbf{u}$, $\mathbf{f}$, and $\boldsymbol{\sigma}$ are the density, velocity, body force, and the stress tensor, respectively. The stress tensor is written as the sum of its isotropic and deviatoric parts:

$$\boldsymbol{\sigma}=-p\mathbf{I}+\mathbf{T}, \quad \mathbf{T}=2\mu\boldsymbol{\varepsilon}(\mathbf{u}), \quad \boldsymbol{\varepsilon}(\mathbf{u})=\frac{1}{2}((\nabla\mathbf{u})+(\nabla\mathbf{u})^T), \tag{3}$$

where p and μ are the pressure and coefficient of dynamic viscosity. Both the Dirichlet and Neumann-type boundary conditions are accounted for, represented as

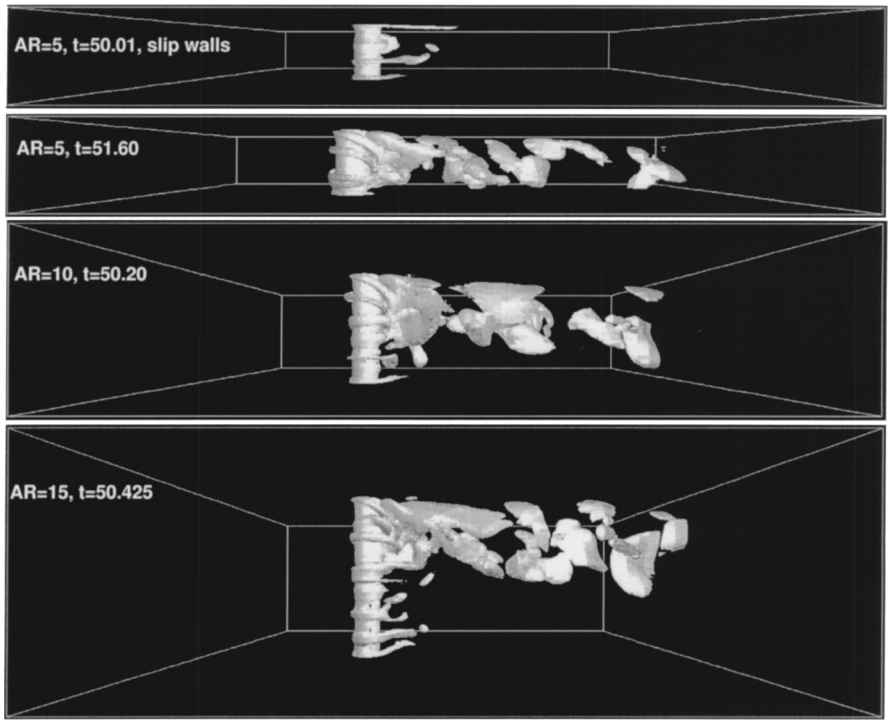

Fig. 4 Re=200, $\alpha=5$ flow past a rotating cylinder: isosurfaces of the spanwise component of vorticity ($=0.4$) for various aspect ratios. The top frame corresponds to the simulation with slip walls as the end condition. For the other three frames, the upper wall is a no-slip wall.

$$\mathbf{u}=\mathbf{g} \text{ on } \Gamma_g, \quad \mathbf{n}\cdot\boldsymbol{\sigma}=\mathbf{h} \text{ on } \Gamma_h, \tag{4}$$

where Γ_g and Γ_h are complementary subsets of the boundary Γ. The initial condition on the velocity is specified on Ω:

$$\mathbf{u}(\mathbf{x},0)=\mathbf{u}_0 \quad \text{on } \Omega, \tag{5}$$

where $\mathbf{u}_0$ is divergence-free.

The force and moment coefficients are computed by carrying an integration, that involves the pressure and viscous stresses, around the circumference of the cylinder:

$$C_D=\frac{1}{\frac{1}{2}\rho U^2 2aL}\int_{\Gamma_{\text{cyl}}}(\boldsymbol{\sigma}\mathbf{n})\cdot\mathbf{n}_x d\Gamma, \tag{6}$$

$$C_L=\frac{1}{\frac{1}{2}\rho U^2 2aL}\int_{\Gamma_{\text{cyl}}}(\boldsymbol{\sigma}\mathbf{n})\cdot\mathbf{n}_y d\Gamma. \tag{7}$$

Here $\mathbf{n}_x$ and $\mathbf{n}_y$ are the Cartesian components of the unit vector $\mathbf{n}$ that is normal to the cylinder boundary Γ_{cyl}, a is the radius of the cylinder, L its spanwise length, U the freestream speed, and C_D and C_L are the drag and lift coefficients, respectively.

The various parameters that influence this flow are Re, α, AR and end conditions. The Reynolds number is defined as $\text{Re}=2Ua/\nu$ where a is the radius of cylinder, U the freestream speed and ν is the coefficient of kinematic viscosity of the fluid. The rotation rate of the cylinder is nondimensionalized with respect to the freestream speed and is given as $\alpha=a\omega/U$ where ω is the angular velocity of the cylinder about its own axis. The aspect ratio, AR, of the cylinder is the ratio of its spanwise length and diameter. All the results presented in this article are with respect to the non dimensional time $\tau=Ut/a$, where t is the actual time.

3 Finite Element Formulation

Consider a finite element discretization of Ω into subdomains Ω^e, $e=1,2,\ldots,n_{\text{el}}$, where n_{el} is the number of elements. Based on this discretization for velocity and pressure, we define the finite element trial function spaces $\mathcal{S}_{\mathbf{u}}^h$ and $\mathcal{S}_p^h$, and weighting function spaces $\mathcal{V}_{\mathbf{u}}^h$ and $\mathcal{V}_p^h$. These function spaces are selected, by taking the Dirichlet boundary conditions into account, as subsets of $[\mathbf{H}^{1h}(\Omega)]^{n_{sd}}$ and $\mathbf{H}^{1h}(\Omega)$, where $\mathbf{H}^{1h}(\Omega)$ is the finite-dimensional function space over Ω. The stabilized finite element formulation of Eqs. (1)–(2) is written as follows: find $\mathbf{u}^h\in\mathcal{S}_{\mathbf{u}}^h$ and $p^h\in\mathcal{S}_p^h$ such that $\forall\mathbf{w}^h\in\mathcal{V}_{\mathbf{u}}^h$, $q^h\in\mathcal{V}_p^h$

$$\int_\Omega \mathbf{w}^h\cdot\rho\left(\frac{\partial\mathbf{u}^h}{\partial t}+\mathbf{u}^h\cdot\nabla\mathbf{u}^h-\mathbf{f}\right)d\Omega+\int_\Omega\boldsymbol{\varepsilon}(\mathbf{w}^h):\boldsymbol{\sigma}(p^h,\mathbf{u}^h)d\Omega$$
$$+\int_\Omega q^h\nabla\cdot\mathbf{u}^h d\Omega+\sum_{e=1}^{n_{\text{el}}}\int_{\Omega^e}\frac{1}{\rho}(\tau_{\text{SUPG}}\rho\mathbf{u}^h\cdot\nabla\mathbf{w}^h+\tau_{\text{PSPG}}\nabla q^h)\cdot$$

$$\left[\rho\left(\frac{\partial\mathbf{u}^h}{\partial t}+\mathbf{u}^h\cdot\nabla\mathbf{u}^h-\mathbf{f}\right)-\nabla\cdot\boldsymbol{\sigma}(p^h,\mathbf{u}^h)\right]d\Omega^e$$
$$+\sum_{e=1}^{n_{el}}\int_{\Omega^e}\tau_{\text{LSIC}}\nabla\cdot\mathbf{w}^h\rho\nabla\cdot\mathbf{u}^h d\Omega^e=\int_{\Gamma_h}\mathbf{w}^h\cdot\mathbf{h}^h d\Gamma. \tag{8}$$

The variational formulation given by Eq. (8), includes certain stabilization terms added to the basic Galerkin formulation to enhance its numerical stability. the first three terms and the right-hand side constitute the Galerkin formulation of the problem. De-

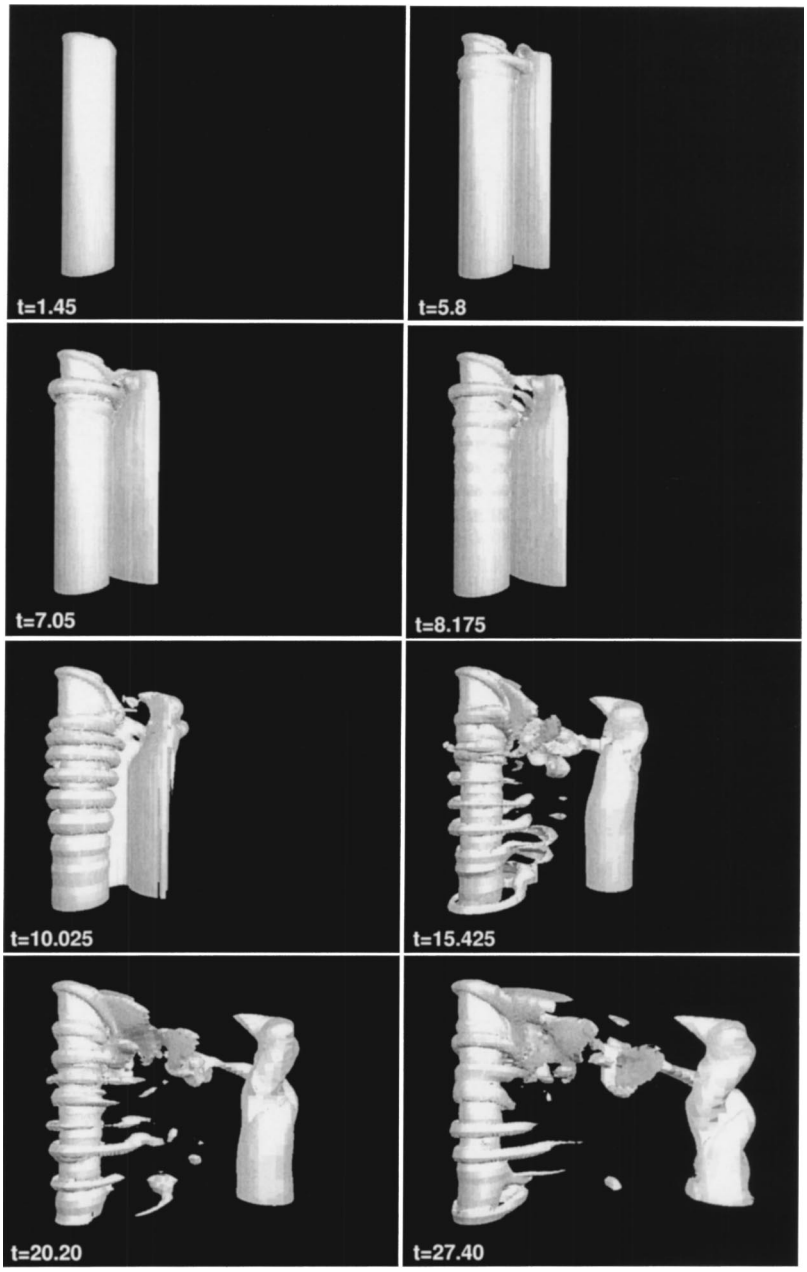

Fig. 5 Re=200, $\alpha=5$, $AR=15$ flow past a rotating cylinder with a no-slip end wall: isosurfaces of the spanwise component of vorticity ($=0.4$) at various time instants following an impulsive start

tails on the formulation can be found in references [13,14]. The stabilization terms involve the use of a characteristic ''element length.'' In the present computations this length is defined as the minimum edge length of an element, [13].

4 Results and Discussions

All the results in this article are for the Re=200 and $\alpha=5$ flow.

4.1 Two-Dimensional Computations. The cylinder resides in a rectangular domain and a flow velocity corresponding to the rotation rate, α is specified on the cylinder surface. The rotation is in the counterclockwise direction. A freestream value is assigned for the velocity at the upstream boundary while, at the downstream boundary, a Neumann-type boundary condition for the velocity is specified that corresponds to zero viscous stress vector. On the upper and lower boundaries, the component of velocity normal to and the component of stress vector along these boundaries is prescribed zero value. The initial condition for all the computations is an impulsive start, i.e., at $t=0$ the velocity is assigned value that corresponds to potential flow past a stationary cylinder. The outer boundaries are located at $100D$ from the center of the cylinder.

Figure 1 shows the fully developed solution obtained from the two-dimensional computations. Clockwise vorticity (negative) on the upper surface and counterclockwise vorticity (positive) on lower surface of the cylinder is generated. The high rotation rate of the cylinder causes this vorticity to move outward as tightly wound spirals. The stability of this flow has been ascertained via linear stability analysis, [2], and also by computing the flow for an eccentric cylinder [10]. Detailed results for $\alpha=5$ and other rotation rates have been presented in Mittal and Kumar [2].

4.2 Three-Dimensional Computations. Very large lift coefficients can be obtained for two-dimensional flows past a cylinder for high rotation rates. Tokumaru and Dimotakis [4] have reported a strong dependence of the lift coefficient on the aspect ratio of the cylinder (ratio of spanwise length to diameter) and its end conditions. To study the same, three-dimensional computations for flow past a rotating cylinder with an impulsive start are carried out for various end conditions and cylinder span-to-diameter ratio. Kalro and Tezduyar [15] used a very similar finite element formulation to study flow past a nonspinning cylinder.

In the three-dimensional simulations the cylinder extends along the entire span of the computational domain. One of the side boundaries, that intersects with the cylinder, is assumed to be a ''no-slip'' wall for the velocity while symmetry conditions are imposed on the other side wall. These boundary conditions simulate a rotating cylinder, without end plates, placed in a tunnel. Only one half of the tunnel is simulated. Mittal [16] investigated the flow past low aspect-ratio nonspinning cylinders in the presence of wall. The aspect ratios considered in the present work are 5, 10, and 15. A computation for $AR=5$ with ''slip'' side walls is also carried out to assess the effect of end conditions. The finite element mesh for the computation with $AR=15$ consists of 284,199 nodes and 270,000 hexahedral elements. At each time-step approximately 1.1 million nonlinear equations are solved iteratively. The time histories of the lift and drag coefficients for these simulations are shown in Fig. 2 along with the results from two-dimensional computations. It is observed that both the end conditions and the cylinder aspect ratio have a significant impact on the aerodynamic coefficients. Compared to the steady-state two-dimensional flow, the ''no-slip'' side wall results in lower lift and higher drag. The lift coefficient reduces with the decrease in aspect ratio of the cylinder. An increase in the aspect ratio of the cylinder reduces the effect of the ''no-slip'' wall. With the ''slip'' end conditions on the velocity on side walls, fairly high lift and low drag coefficients are obtained with a low aspect-ratio cylinder ($AR=5$). This study brings out the effect of end conditions in such flows. A similar observation was reported by Tokumaru and Dimotakis [4].

Shown in Fig. 3 are the spanwise averaged C_p distributions for the various three-dimensional computations at approximately $t=50$. It is well known that for a stationary cylinder, the surface pressure distribution for the viscous and potential flows are qualitatively different. This is attributed to the flow separation in the case of a real fluid. However, for a rotating cylinder spinning at $\alpha=5$, it is interesting to observe that the pressure distributions for the two-dimensional and potential flows are very similar, qualitatively. As expected, compared to the two-dimensional flow, the three-dimensional effects tend to reduce the suction generated on the cylinder. Among all the cases, the C_p variation for the $AR=5$ case with slip walls is the closest to that from the two-dimensional computations. The peak suction decreases as the AR is reduced. It is also observed that the location of the peak value of C_p moves towards the front of the cylinder as AR is reduced and end effects become important.

Figure 4 shows the isosurfaces for the spanwise component of the vorticity for various cases at approximately $t=50$. In all the cases centrifugal instabilities, such as those observed in flows between two concentric rotating cylinders, exist along the span of the spinning cylinder. The spanwise wavelength of these centrifugal instabilities is, approximately, one cylinder diameter which is similar to that observed in Taylor instabilities. In addition, interaction of the rotating cylinder with the boundary layer on the ''no-slip'' side wall leads to flow separation. Both these effects contribute to a loss in lift and increase in drag. The effect of the side wall reduces as one moves away from it. For example, for $AR=15$, the flow on the lower half of the span appears quite similar to the $AR=5$ flow with slip walls. Therefore, for a cylinder with very large aspect ratio the aerodynamic coefficients may be quite close to those for the two-dimensional flows. However, the three-dimensional centrifugal instabilities would still be present and lead to loss of lift and increase in drag, compared to the two-dimensional flow.

Figure 5 shows the isosurfaces for spanwise vorticity at various time instants for $AR=15$. It is interesting to note that, as was the case with two-dimensional computations, only one spanwise vortex (the startup vortex) is shed for $\alpha=5$. The development of the centrifugal instabilities along the cylinder span can also be observed in the figure. Their initial development seems to be instigated by the end conditions. The shear generated by the boundary layer on the side wall is also responsible for the twisting of the startup vortex. The end effects can be eliminated/minimized by using end plates. Prandtl observed a value of $C_L \sim 3.2$ for a cylinder of $AR=4.7$ and at $\mathrm{Re}=5.2\times10^4$ (as reported by Tokumaru and Dimotakis [4] and Goldstein [3]). However, on using end plates of diameter 1.7 times the cylinder diameter, he observed that the value of the lift coefficient goes up to, approximately, 5.

Very high lift coefficients are observed for high rotation rates of the cylinder. The present results support the observation by Tokumaru and Dimotakis [4] that Prandtl's limit does not hold for large aspect-ratio cylinders. It certainly does not hold for the two-dimensional flows. The lift coefficient from the two-dimensional computations approach the values from the three-dimensional setup for large aspect-ratio cylinders.

5 Concluding Remarks

Three-dimensional flow past a cylinder, rotating in the counterclockwise sense, and placed in uniform stream ($\mathrm{Re}=200$) has been analyzed for a spin rate corresponding to $\alpha=5$. A stabilized finite element method is utilized to solve the incompressible Navier-Stokes equations in the primitive-variables formulation.

It is found that the aspect ratio of the cylinder (spanwise length/diameter) and its end conditions play an important role in determining the amount of lift generated by the rotating cylinder. While the two-dimensional flow for $\alpha=5$ is stable, the three-dimensional flow is associated with centrifugal instabilities. These instabilities are observed even for the case with ''slip walls'' and are quite similar to those observed in flow between rotating cylinders. The presence of a no-slip side wall (no end plates) results in flow separation. Both of these effects contribute to loss of lift and increased drag as compared to a purely two-dimensional flow. It is found that very large lift coefficients can be realized for large aspect-ratio cylinders via the Magnus effect and that Prandtl's limit does not hold.

Acknowledgment

Partial support for this work has come from the Department of Science and Technology, India.

References

[1] Prandtl, L., 1925, ''The Magnus Effect and Windpowered Ships,'' Naturwissenschaften, **13**, pp. 93–108.
[2] Mittal, S., and Kumar, B., 2003, ''Flow Past a Rotating Cylinder,'' J. Fluid Mech., **476**, pp. 303–334.
[3] Goldstein, S., 1938, *Modern Developments in Fluid Dynamics*, Clarendon Press, Oxford, UK.
[4] Tokumaru, P. T., and Dimotakis, P. E., 1993, ''The Lift of a Cylinder Executing Rotary Motions in a Uniform Flow,'' J. Fluid Mech., **255**, pp. 1–10.
[5] Chew, Y. T., Cheng, M., and Luo, S. C., 1995, ''A Numerical Study of Flow Past a Rotating Circular Using a Hybrid Vortex Scheme,'' J. Fluid Mech., **299**, pp. 35–71.
[6] Glauert, W. B., 1957, ''The Flow Past a Rapidly Rotating Circular Cylinder,'' Proc. R. Soc. London, Ser. A, **242**, pp. 108–115.
[7] Chen, Yen-Ming, Ou, Yuh-Roung, and Pearlstein, A. J., 1993, ''Development of the Wake Behind a Circular Cylinder Impulsively Started Into Rotary and Rectilinear Motion,'' J. Fluid Mech., **253**, pp. 449–484.
[8] Badr, H. M., Coutanceau, M., Dennis, S. C. R., and Menard, C., 1990, ''Unsteady Flow Past a Rotating Cylinder at Reynolds Numbers 10^3 and 10^4,'' J. Fluid Mech., **220**, pp. 459–484.
[9] Mo-Hong, Chou, 2000, ''Numerical Study of Vortex Shedding From a Rotating Cylinder Immersed in a Uniform Flow Field,'' Int. J. Numer. Methods Fluids, **32**, pp. 545–567.

[10] Mittal, S., 2001, ''Flow Past Rotating Cylinders: Effect of Eccentricity,'' ASME J. Appl. Mech., **68**, pp. 543–552.
[11] Mittal, S., 2001, ''Control of Flow Past Bluff Bodies Using Rotating Control Cylinders,'' J. Fluids Struct., **15(2)**, pp. 291–326.
[12] Stansby, P. K., and Rainey, R. C. T., 2001, ''A CFD Study of the Dynamic Response of a Rotating Cylinder in a Current,'' J. Fluids Struct., **15**, pp. 513–521.
[13] Tezduyar, T. E., Mittal, S., Ray, S. E., and Shih, R., 1992, ''Incompressible Flow Computations With Stabilized Bilinear and Linear Equal-Order-Interpolation Velocity-Pressure Elements,'' Comput. Methods Appl. Mech. Eng., **95**, pp. 221–242.
[14] Mittal, S., 2000, ''On the Performance of High Aspect-Ratio Elements for Incompressible Flows,'' Comput. Methods Appl. Mech. Eng., **188**, pp. 269–287.
[15] Kalro, V., and Tezduyar, T. E., 1997, ''Parallel 3D Computation of Unsteady Flows Around Circular Cylinders,'' Parallel Comput., **23**, pp. 1235–1248.
[16] Mittal, S., 2001, ''Computation of 3D Flows Past Circular Cylinders of Low Aspect Ratio,'' Phys. Fluids, **13**, pp. 177–191.